Analyzing laser-plasma interferograms with the Continuous Wavelet Transform technique

P. Tomassini, A. Giulietti and L.A. Gizzi

Istituto di Fisica Atomica e Molecolare
CNR Area della Ricerca di Pisa
Via V. Alfieri 1 Ghezzano (Pisa)

November 15, 2000

Abstract

Laser-plasma interferograms are currently analyzed by extracting the phase-shift map with FFT techniques. This methodology works well when interferogram images are marginally corrupted by noise and reduction of fringe visibility, but it frequently fails when dealing with low-quality images.

In this note we will present a novel approach to the phase-shift map computation procedure which makes an extensive use of the Continuous Wavelet Transform tool. We compare the performances of the new technique, which will call **IACRE** *, "Interferogram Analysis by Continuous wavelet trasform Ridge Extraction", with the standard FFT-based one analyzing four different interferograms. We will show that such a new procedure is considerably more robust than the FFT-based one, particularly in the case of strongly noisy fringe patterns.*

We will also shortly describe the original "Integrated Laser-Plasma Inteferogram Analyzer" software developed by our group, by which it is possible to analyze laser-plasma interferograms by using both the FFT-based and IACRE methods to extract phase-shifts and to compute the electronic density in the case of cylindrical symmetry.

1 Introduction

Interferometric techniques are widely used to characterize the physical properties of a variety of optical media. An important class of applications concerns the investigation of the density distribution of plasmas produced by high power laser-matter interactions. In recent years various interferometer schemes have been developed and successfully applied to the characterisation of the wide range of plasma condition which can be achieved in laser-plasma experiments, from the long-scalelength underdense plasma generated by laser explosion of a thin foil target to the steep, denser plasma generated by short pulse interaction with a solid target. All these schemes make use of a so-called probe beam which consists of a laser pulse which probes the plasma at a given time. In one of these schemes, referred to as the modified Nomarski interferometer [1][2] [3], a portion of this beam propagates through the plasma and carries the phase shift information. Finally this portion of the beam is made to interfere with an unperturbed portion to generate a fringe pattern. The fringe pattern must be then analysed to obtain the two-dimensional phase-shift which contains the physical information on the plasma. Then, provided that appropriate symmetry conditions are satisfied, inversion techniques can be applied to the phase shift pattern to obtain the density profile.

The simplest way of reading a fringe pattern consists in building a grid over the pattern and in measuring, for each position on the grid, the number of fringe jumps with respect to the unperturbed fringe structure. This procedure is very simple and can be performed manually. However, the amount of information which can be extracted in this way is very limited due to the small number of grid points that can be employed.

In 1982 a novel fringe analysis technique was proposed [4] in which the phase extraction was carried out using a procedure based upon Fourier transform. This technique allows the information carried by the fringe position on the film to be decoupled by spatial variations of the background intensity as well as by variations in the fringe visibility, provided that the scalelength of such perturbations is large compared to the fringe separation. A few years later this FFT technique was applied for the first time to laser-produced plasmas [5]. More recently the technique was extensively applied by our group to the analysis of long-scalelength underdense laser-plasmas [6] In recent years great advances in the interferometry of laser-plasmas has been achieved using sub-picosecond probe pulses. The use of short pulses as probes has the great advantage of reducing dramatically of the fringe-smearing effect due to the motion of the plasma during the probe pulse. This scheme was successfully carried out to investigate short-lived phenomena in the propagation of ultra-short laser pulses with plasmas [7]. The extensive use of the FFT based technique carried out by our group has shown that this technique is in general fast and very effective. In some circumstances however, when short probe pulses are used, background noise and reduced fringe visibility make the FFT based analysis technique unstable and the results are not fully satisfactory and more robust analysis techniques are needed.

In this report we show that Continuous Wavelet Transform can be successfully applied to the analysis of interferograms resulting in a much more flexible and reliable than the FFT based technique. To our knowledge, this is the first time that a Continuous Wavelet Transform approach is applied to fringe pattern analysis and in particular to interferometric analysis in laser-produced plasmas.

In section 2 we will shortly introduce the Continuous Wavelet Transform (CWT), stressing its remarkable properties of good space-scale analyzer.

In section 3 we introduce the *IACRE* tool and we compare its performance with the FFT-based one.

In section 4 we shortly describe the software implementation of the new method developed by our group: a Graphics Interface integrated tool running under MATLAB.

Section 5 is devoted to comments and further activity description.

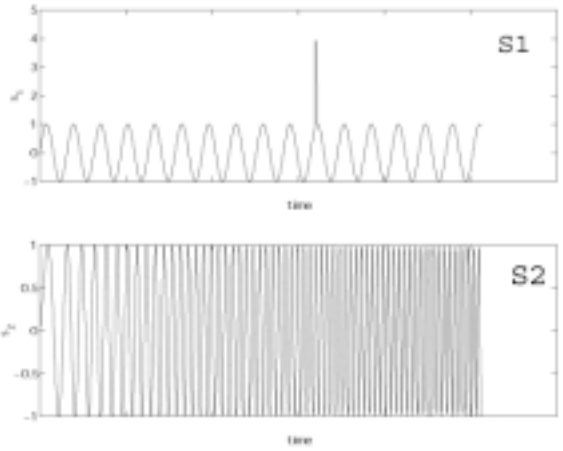

Figure 1: *The signal s_1: a sinusoid with a well localized event. The signal s_2: a frequency-modulated sinusoid.*

2 A short introduction to Continuous Wavelet Analysis

2.1 The need for a time-frequency analysis

The Continuous Wavelet Transform is a tool to obtain a signal representation which is intermediate between the "real time" description $s = s(t)$ and the "spectral" description $\hat{s} = \hat{s}(\omega)$, so that it is a very powerful tool to obtain a space-scale (or time-frequency) description of a sequence of data.

The need of a time-frequency description of a sequence is much strong in cases of well-localized events in the signal or when the signal represents a sum of frequency-modulated components (as for each section of an interferogram image (see section 4). Consider for example the two signals(see figure Fig. 1):

$$\begin{aligned} s_1 &= \sin\left((2\pi t) + a\,\delta(t - t_0)\right), \\ s_2 &= \sin\left((2\pi t)(1 + b\,\sqrt{t})\right). \end{aligned} \tag{2.1}$$

Apart from the presence of a "jump" at time t_0, the first signal is a pure sinusoid. The second signal, instead, is a frequency-modulated sinusoid. What's about FFT coefficients? What can be learned from them? Let's look Fig. 2; the module of the FFT coefficients for s_1 tells us that the main component of the signal is a sinusoid (the sharp peak), but nothing can be inferred about the departure of the signal from a pure sine: neither if such departure is periodic nor, if

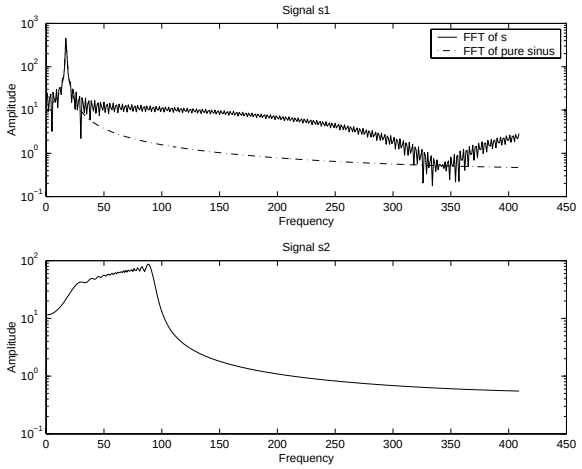

Figure 2: *Fast Fourier Transform of s_1 and s_2. The dashed line in the top frame represents the module of the FFT coefficients for a pure sinus.*

not, if it is well localized in time (and consequently at which time is concentrated). The modulus of the FFT coefficients for s_2 are even less helpful in suggesting us the structure of the signal: a broad band of frequencies is present and no main frequency can be found. These simple examples show that a "full spectral" analysis could be unsatisfactory if we are interested in the knowledge of both the spectral contain and time structure of a signal.

The obvious step that can be made to overcome the lack of time sensitivity is the introduction of a sequence of windows of a given width and centered at different times: for each window the FFT of the signal is computed and a partial time resolution is obtained. These techniques are called "Short-Time Fourier Transform" or "Windowed Fourier Transform" or "Gabor Transform" [9]. The Gabor Transform is currently used in many context but is not considered by the signal-processing community a "full analysis tool". This is because the number of oscillations of each sinus in the window depends on the frequency and consequently the spectral and spatial resolutions should be optimized (by tuning the window length) only in a narrow band.

From the early 80's, with the introduction of the Wavelet Transform, a satisfying time-frequency analysis tool is available [10] [11] [12].

2.2 The Continuous Wavelet Transform

To introduce the Wavelet Transform, let us first define notations for the Fourier Transform. For a signal $s \in L^1(\mathcal{R}) \cap L^2(\mathcal{R})$ the Fourier coefficients, that is the scalar product between the signal and the infinitely oscillating terms $e_\omega = e^{-i\,\omega t}$:

$$\hat{s}(\omega) \equiv < e_\omega | s > = \int_{-\infty}^{\infty} dt e^{-i\,\omega t} s(t) \qquad (2.2)$$

form a complete basis of the space to which s belongs and an inverse Fourier transform can be applied to $\hat{s}(\omega)$ to recover s: $s(t) = \int_{-\infty}^{\infty} d\frac{\omega}{2\pi} e^{i\,\omega t} \hat{s}(\omega)$.

Let us introduce a function $\Psi(t)$ called *Mother wavelet*. Now, instead of decomposing the signal s as a sum of the pure oscillating terms e_ω (*Fourier Transform*), we build a decomposition of s **in terms of the base of all the translated** (with parameter b) bf and scaled (with parameter a) Ψ (*Continuous Wavelet Transform*). The basis of the Continuous Wavelet Transform (*CWT*) is than a two-parameter family of functions

$$\Psi_{a,b}(t) \equiv \frac{1}{a} \Psi \left(\frac{(t-b)}{a} \right) . \qquad (2.3)$$

The choice of the Mother Wavelet used to build the analyzing base is quite free (with a restriction that will be shown below) and must be adapted to the actual information that should be extracted from the signal. This is an important topics that the reader may deepen with the help of reference [11].

Once the two-parameter base has been built, one can compute the CWT coefficients as

$$\begin{aligned} W_s(a,b) \quad &\equiv \quad < \Psi_{a,b} | s > \qquad (2.4) \\ &= \quad \int_{-\infty}^{\infty} dt \frac{1}{a} \overline{\Psi \left(\frac{(t-b)}{a} \right)} s(t), \\ (\quad [a,\,b] \quad &\in \mathcal{R},\ a > 0 \ ) \end{aligned}$$

or, with the help of Fourier Transform, as [11]

$$W_s(a,b) = \frac{1}{2\pi} \int_{-\infty}^{\infty} d\omega \overline{\hat{\Psi}}(a\,\omega) e^{i\,\omega\,b} \hat{s}(\omega) . \qquad (2.5)$$

If the Mother Wavelet Ψ has zero mean (*admissibility condition*), than an inversion algorithm can

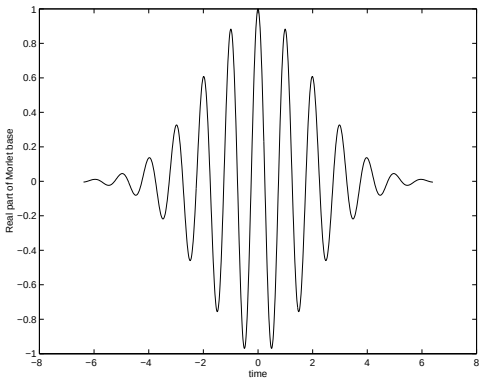

Figure 3: *The real part of Morlet Mother Wavelet.* $\omega_0 = 2\pi; \tau = 4$.

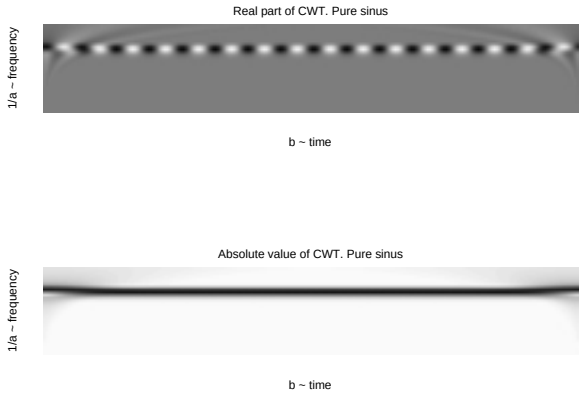

Figure 4: *The real part and absolute value CWT maps of a pure sinus with Morlet Mother Wavelet.*

be applied [12]; the simpler procedure to recover the signal s from its Wavelet transform is the so-called "Morlet inversion formula"

$$s(t) = \frac{1}{k_\Psi} \int_0^\infty W_s(a,b) \frac{da}{a} \tag{2.6}$$

where it is assumed that

$$k_\Psi = \int_0^\infty \overline{\hat{\Psi}(a\xi)} \frac{da}{a}$$

is finite, nonzero and independent on ξ.

In the subset of admissible wavelets, "Morlet-family" wavelets are largely used in studying signals with strong components of pure sinus or modulated sinusoids. The Morlet base has the form

$$\Psi(t) = e^{i\,\omega_0 t}\; e^{-(t/\tau)^2}\,, \tag{2.7}$$

where the parameters ω_0 and τ control the peak frequency and the width of the wave respectively. The product $\omega_0 \times \tau$ *controls the time and spectral resolution of the Wavelet decomposition*: a large τ corresponds to a long wave (high spectral resolution and low temporal resolution) while a small τ produces an "event based" analysis (low spectral resolution and high temporal resolution).

We now face the problem of a numerical computation of the Wavelet coefficients map $W_s(a,b)$. For a sequence of N samples $s_i;\ i = 1...N$ of s, the translation parameter b (which controls the central position of the wave envelope) can be sampled in a straightforward way: $b \to b_i;\ i = 1...N$. The scaling parameter a (which controls the characteristic scale of the wave) may be sampled in two main ways:

- **Linear frequency sampling:** $\frac{2\pi}{a_j} = k_1 + \frac{j}{M} k_2 - k_1;\ j = 1...M$, where k_1 and k_2 are the lower and upper wave vectors which are analyzed.
- **Natural sampling or Log sampling:** $a_j = 2^{-j/N_v}\ j = 1...M$, where N_v is the "number of voices per octave" parameter. Each a_j is called "voice" and, in the case $N_v = 12$, Log sampling exactly corresponds to the spectral sampling of musical tones in the "tempered scale" introduced by J.S. Bach [16]

The Log sampling of CWT coefficients in the Morlet basis is very useful when the spectral content of the signal is the main information to be extracted, because it provides a good compromise between spatial and spectral resolution. As the reader can easily check, the spectral resolution at each voice is proportional to the peak frequency of the voice $\left(\frac{\omega_0}{a}\right)$ so that the relative spectral uncertainty $\frac{\Delta f}{f}$ is constant along the a axes.

To familiarize with the CWT map, we compute the CWT coefficients of a pure sine signal. Figure Fig. 4 shows both the real part and the absolute value of CWT coefficients in the Log sampling ($N_v = 24$). In these figures CWT maps are organized with "frequencies" increasing from the top to the bottom. The absolute value of CWT map is almost zero, apart from a thin horizontal band centered at a scale corresponding to the input signal frequency: Continuous

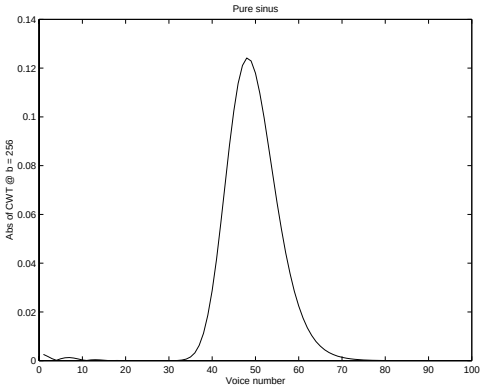

Figure 5: *The absolute value CWT map of a pure sinus of Morlet Mother Wavelet: a zoom @b constant.*

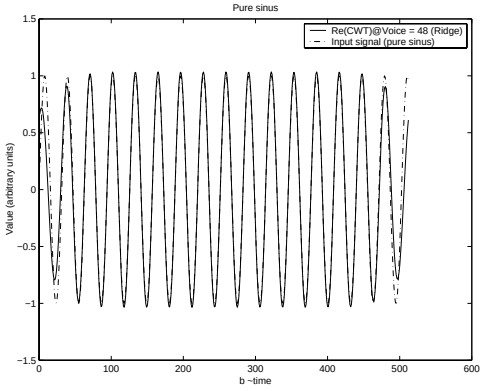

Figure 6: *The sequence of real part of CWT map of a pure sinus with Morlet Mother Wavelet @ Ridge.*

Wavelet Transform may be a good spectral analyzer even for perfectly periodic signals [16] (see also Fig. 5 in which a "zoom", that is a section of the absolute value of CWT map at $b = const.$, is shown).

The real part of CWT map shows a second important feature of CWT with Morlet (or generally with progressive) basis: $\mathcal{R}(W_s)$ is almost constant, apart from the thin band centered at the signal frequency. The sequence

$$R_s(b) \equiv \mathcal{R}(W_s)(b, a_R(b)) \tag{2.8}$$

where for each b^* $a_R(b^*)$ is the voice corresponding to a local maximum of the zoom of $abs(CWT)$ at $b = b^*$, well reproduces the input signal itself, as is shown in Fig. 6.

The sequence (ore more generally the sequences when more complex signals are analyzed) 2.8 is called *the Ridge of CWT map* and represents the subset of CWT map where most of the "energy" is contained. To familiarize with Ridge properties, let us consider a signal of the form:

$$s(t) = A(t)\, \cos(\phi(t)) \tag{2.9}$$

where $A(t)$ is assumed be slowly varying with respect to the oscillations, that is

$$\frac{1}{A}\frac{dA}{dt} << \phi' \,.$$

If Ψ is a progressive Wavelet, then with straightforward computations including "stationary phase methods" we have (see [14] and [13])

$$W_s(a,b) \approx \frac{1}{2} A(b) e^{i\,\phi(b)}\, \overline{\hat{\Psi}(a\phi'(b))} \,. \tag{2.10}$$

Since $\hat{\Psi}$ is centered at $\omega = \omega_0$, $\hat{\Psi}(a\phi'(b))$ is not negligible if

$$a \approx a_R(b) \equiv \frac{\omega_0}{\phi'(b)} \tag{2.11}$$

which means that the energy of the CWT map is localized around a thin curve, the *Ridge* curve. To conclude, it is interesting to note that the "instantaneous frequency", that is the time derivative of the phase $\phi(t)$

$$\Omega(t) \equiv \phi'(t) \,,$$

can be easily extracted from the Ridge curve: for each b, as corollary of (2.10), $a_R(b)$ is linked to Ω as

$$\Omega(b) = \frac{\omega_0}{a_R(b)} \,.$$

Let us now compare FFT and CWT analysis of signals s_1 and s_2 (figure Fig. 1). The CWT map of signal $s1$ is reproduced in Fig. 7. Unlike FFT map, in Fig. 7 is evident that the signal s_1 is something like a pure sine of measurable frequency plus some localized event at a detectable time t_0. In addition, since the shape of the CWT of the most localized inputs are well known, on can easily recognize that the event is similar to a *delta* shot.

The analysis of the CWT map of signal s_2 (see Fig. 8) is more interesting for our scope. The map shows a single ridge, then a single frequency-modulated

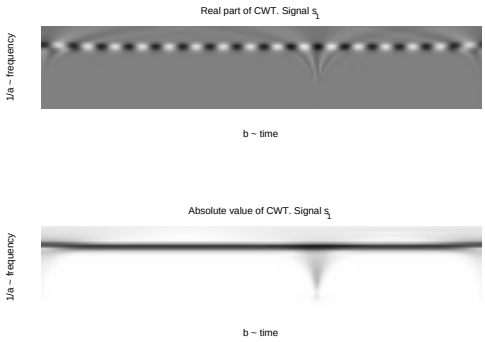

Figure 7: *The real part and absolute value CWT maps of a signal $s1$ with Morlet Mother Wavelet.*

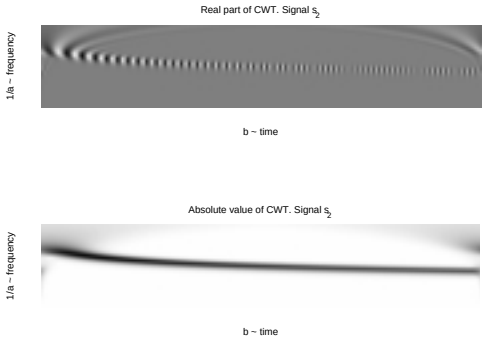

Figure 8: *The real part and absolute value CWT maps of a signal $s2$ with Morlet Mother Wavelet.*

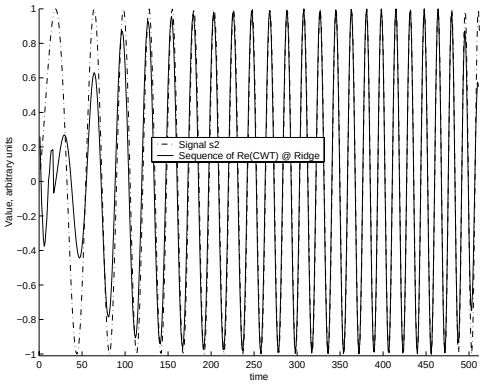

Figure 9: *The sequence of real part of CWT map of signal $s2$ with Morlet Mother Wavelet @ Ridge*

signal is present with instantaneous frequency $\Omega(b)$ increasing with time. The Ridge sequence $R_{s2}(b) \equiv \mathcal{R}(W_{s2})(b, a_R(b))$ is shown in Fig. 9 and it is compared with the input signal $s2$ itself. Apart from boundary-generated errors, the Ridge sequence well reproduces the input signal; *this means that the Ridge CWT sub-map succeed in capturing the signal characteristics as for example instantaneous intensity, phase and frequency.* This is the main characteristic of CWT analysis which will constitute the core of the *IACRE* interferograms analysis (see next section).

2.3 Noisy data

We now face one of the most relevant problems in signal processing: the identification and (eventually) the parameters estimation of a noisy signal. Ridge analysis of CWT map plays a rising role in signal processing, especially in the search of non-stationary signals with a very low SNR ratio (see [15] and references therein).

To explore CWT performances in the presence of noisy data, we add gaussian noise to signal $s2$ (see Fig. 10) and compute the CWT map (Fig. 11). The presence of noise (in this case at SNR $= 0.8$) does not destroy the Ridge structure and the resulting Ridge detection gives rise to the sequence $R_{s2+noise}(b) \equiv \mathcal{R}(W_{s2+noise})(b, a_R(b))$ reproduced in Fig. 12. As it is clear in Fig. 12 the Ridge sub-map well captures the "true" input signal even in the presence of a quite strong noise. This is the reason why one of the applications of Wavelet Transform is the denoising of one dimensional data. *To conclude, we stress*

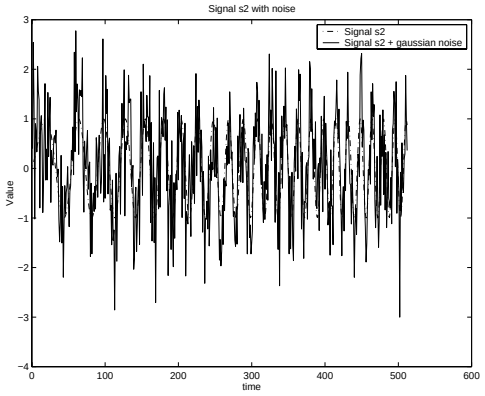

Figure 10: *The signal s2 with gaussian noise added (SNR = 0.8) .*

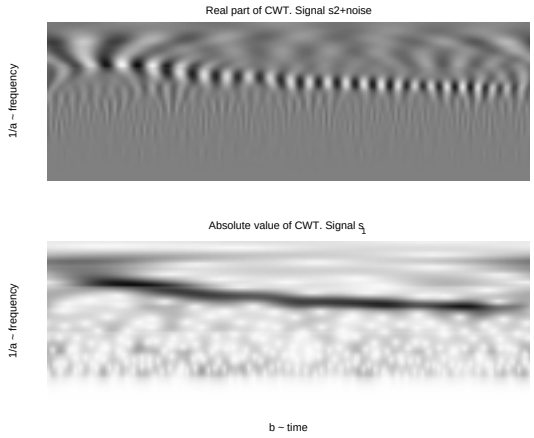

Figure 11: *The real part and absolute value CWT maps of a signal* $s2 + noise$ $(SNR = 0.8)$ *with Morlet Mother Wavelet.*

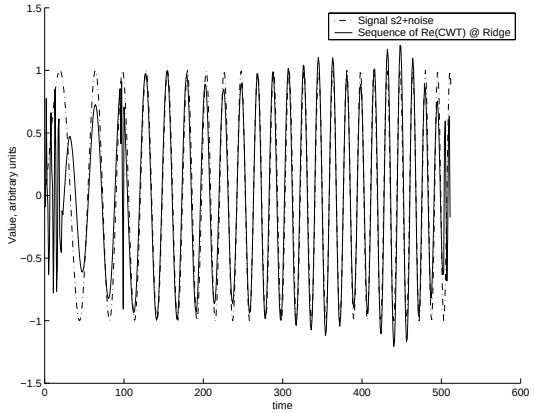

Figure 12: *The sequence of real part of CWT map of signal* $s2$*+noise with Morlet Mother Wavelet @ Ridge (SNR = 0.8) .*

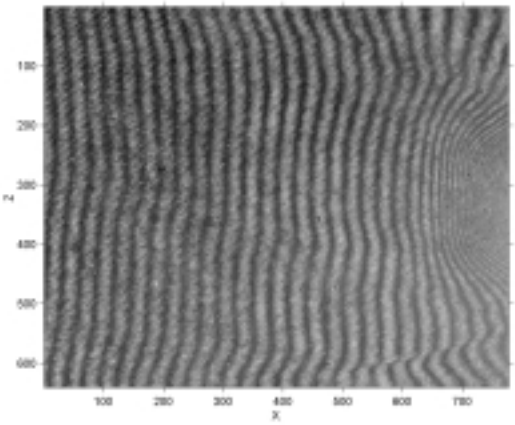

Figure 13: *A sample interferogram* **Int1** *of a plasma produced by laser explosion of a* $0.5\mu m$ *thick,* $400\mu m$ *diameter Aluminium dot coated onto a* $0.1\mu m$ *plastic stripe support. The interferogram was taken* $3.0ns$ *after the peak of the plasma forming pulses using a modified Nomarski interferometer. The intensity on target was* $8.5 \times 10^{13} W/cm^2$*. The probe pulse-length was* $100ps$ *and the probe wavelength was* $0.53\mu m$*. For details on the experimental set-up see [6]*

that the extraction Ridge sequence of the CWT map constitutes a complete and robust method to **denoise and identify** *a sequence made by (eventually a sum of) frequency-modulated harmonic terms.*

3 Comparison between the FFT-based and the *IACRE* methods to extract phase-shift map from interferograms

3.1 The FFT-based method for phase-shift estimation

The extraction of phase-shift map, that is the computation for each pixel of an interferogram image of the phase-shift with respect to a unperturbed wave profile, is usually performed with the help of Fast Fourier Transform (FFT-based method). Consider for example the interferogram of Fig. 13, whose gray-level map be $I(z, x)$ and for each Z build the sequence $s_Z \equiv I(z = Z, x)$ (that is a horizontal sec-

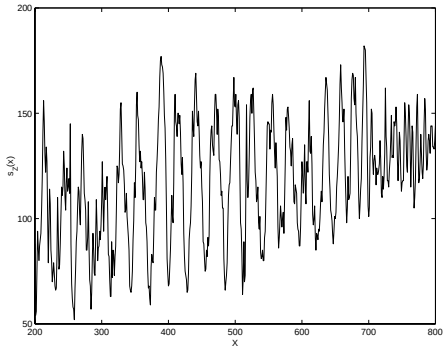

Figure 14: *A section of the interferogram* **Int1** *at* $Z = 400$ *(***bulk***).*

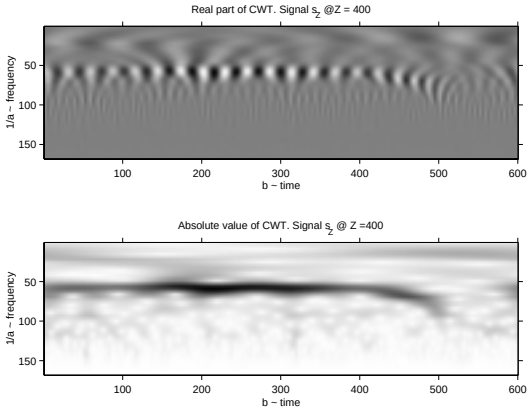

Figure 15: *The real part and absolute value CWT maps of a signal* $s_Z \,@\, Z = 400$ *with Morlet Mother Wavelet.*

tion of the figure). For a unperturbed interferogram image the sequences s_Z should be similar to pure oscillating terms plus noise and (eventually) a slowly varying background. If the departure of such a behaviour is identified as a local frequency modulation of the oscillating term, than the phase-shift $\delta\phi(z, x)$ can be easily computed as the difference between the "true" phase at each x position and the corresponding phase of the not-perturbed sequence. Figure Fig. 14 shows a sequence s_Z for $Z = 400$ (the middle of the frame). The behaviour of s_Z can be identified as a frequency-modulated oscillation with local frequency $\Omega(x)$ increasing with x, plus noise and slowly rising background. In addition, the amplitude of oscillations sharply reduces for $x \approx 700$ (this phenomenon is known as "reduction of fringe visibility", see [6]).

The FFT-based phase-shift extraction uses FFT for both filtering the sequence from noise and background (with cuts in the spatial frequency domain introduced by hand) and extracting the phase by using straightforward FFT coefficients manipulations [6].

3.2 The *IACRE* phase-shift estimation: an introduction

To introduce the *IACRE* method to extract the phase-shift, let us observe that the sequence s_Z (and generally each sequence $I(z = Z, x)$) has the same structure of the signal $s2$, that is a frequency-modulated sequence plus some corrections (noise, slowly varying background). It is then therefore natural to try to extract the s_Z phase-shits by using CWT techniques, with Ridge detection playing a relevant role.

Consider the CWT map of the sequence $s_Z \,@Z = 400$ (see Fig. 15); its aspect is similar to the CWT map of the $s2$ signal (Fig. 8), apart from the presence of a background (a large spot on small frequencies, that is on the top of the map) and a reduction of the Ridge intensity for $x \approx 700$. We can than try to apply the Ridge-extraction technique to the CWT map of s_Z to both denoise the sequence and extract the phase for each pixel position x. The Ridge sequence will be constituted by only the frequency-modulated components of s_Z, so that noise and background will be automatically discarded. This is the case for $s_Z \,@Z = 400$, as it is clear in Fig. 16 and in the zoom on the right hand tail (Fig. 17). The phase sequence $\phi_Z(x)$ for the analyzed array s_Z is then simply computed as the phase of the complex sequence of CWT at the Ridge:

$$\phi_{s_Z}(x) \equiv phase\left((W_{s_Z})(x, a_R(x))\right) , \qquad (3.12)$$

and the phase-shift $\delta\phi_{s_Z}(x)$ is obtained as

$$\delta\phi_{s_Z}(x) \equiv \phi_{s_Z}(x) - \phi_0(x) , \qquad (3.13)$$

where $\phi_0(x) = k_p\, x$ and k_p is the wavenumber of the not-perturbed fringes.

3.3 The *IACRE* method step-by-step

Let us now examine the recipe for the *IACRE* algorithm. Let Be $I(z, x)$ the gray-level image matrix of

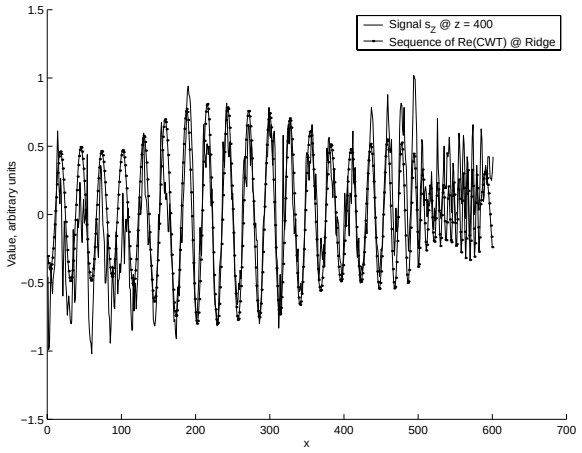

Figure 16: *The sequence of real part of CWT map of signal* $s_Z@Z = 400$ *with Morlet Mother Wavelet @ Ridge.*

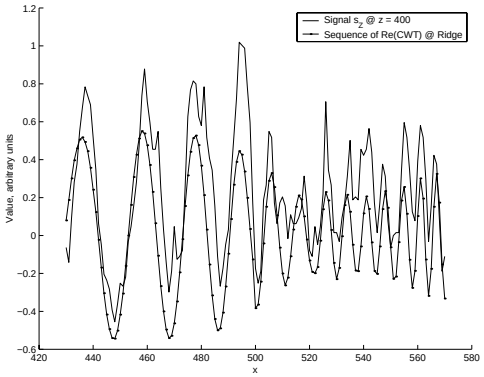

Figure 17: *The sequence of real part of CWT map of signal* $s_Z@Z = 400$ *with Morlet Mother Wavelet @ Ridge. Zoom on the right hand tail.*

dimension $M \times N$. The first steps are the estimation of the unperturbed fringe wavelength k_p and (eventually) image filtering to slightly reduce noise. Next for each $Z \in [1\,M]$ we consider the sequence

$$s_Z(x) \equiv I(z = Z, x)\ , x \in [1\,N]$$

and:

- (I) **Compute the (complex) CWT map**

  $$W_Z(a, b)$$

  with the Morlet base in the Log sampling. To do this one must choose the number of voices per octave N_v. A large N_v ($N_v > 12$) should be preferred if fast changes in the local frequency $\Omega(x)$ are expected. In addition, if we expect that in some regions the local frequency $\Omega_Z(x)$ could have abrupt changes (local irregularities, structures, edges ...), a higher spatial resolution is preferred ($\omega_0 = 2\pi$, $\tau < 1$), while for regular behaviour (like the one of interferogram *Int 1*) a medium space-frequency resolutions should be used ($\tau = 1$).

- (II) **Detect the (complex) Ridge sequence** $R_Z(x) \equiv W_{s_Z}(x, a_R(x))$.

- (III) **Compute the phase of** R_Z:

  $$\phi_Z(x) = phase(R_Z(x))\,.$$

- (IV) **Estimate the phase-shift at** $z = Z$ **as**

  $$\delta\phi(Z, x) \equiv \phi_Z(x) - k_p\,.x$$

The result is a phase-shift matrix $\delta\phi(z, x)$ of dimension $M \times N$. Phase unwrapping algorithms are then applied to the phase-shift map to eliminate unphysical phase jumps (this is the case for FFT-based results too).

3.4 *IACRE* results *versus* FFT-based results

Let us apply the method to the whole interferometric image Fig. 13. The first result is obtained with the *undenoised image*, $N_v = 12$ voices per octave (low N_v). The phase shift matrix is shown in Fig. 18, which should be compared with the FFT-method

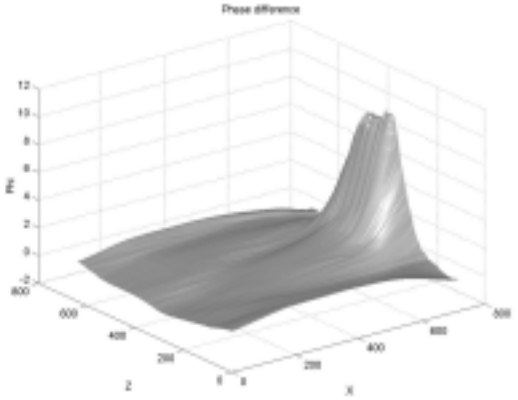

Figure 18: *The phase-shift map (in 2π units) of the not filtered* **Int1** *image Fig. 13.* **CWT method**

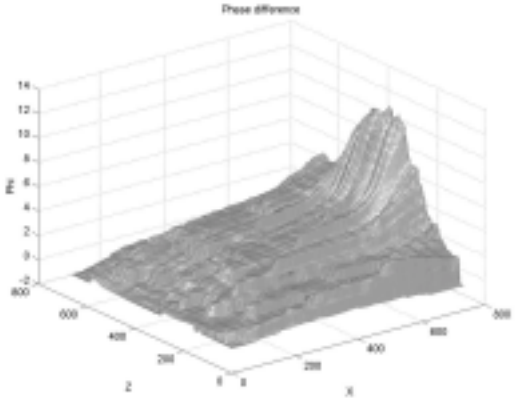

Figure 19: *The phase-shift map (in 2π units) of the not filtered Int1 image Fig. 13.* **FFT method**

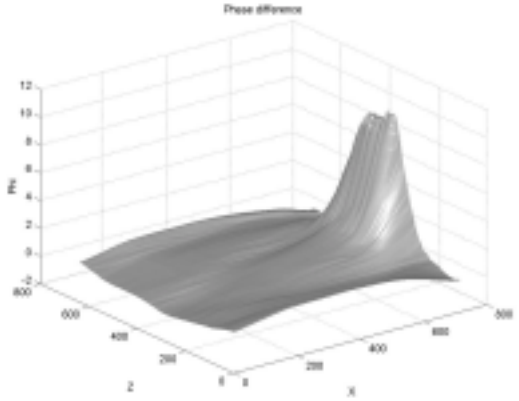

Figure 20: *The phase-shift map (in 2π units) of the of the Median-filtered (3×3)+ Wiener-filtered (5×5)* **Int1** *image Fig. 13.* **CWT method**

phase-shift map of Fig. 19. As is clear from the figures, the *IACRE* method succeeds in generating a clear phase-shift map for the unfiltered image Fig. 13, while the with FFT-based method the output is unsatisfactory because it presents several unphysical phase jumps.

In the next two figures, see (Fig. 20) and (Fig. 21), we compare the performances of CWT and FFT based methods for the same interferogram *now partially filtered from noise* with a Median-Filter of mask size 3×3 pixels followed by a Wiener-Filter 5×5. While the CWT output seems to be good (and basically identical to the not denoised image), FFT output still remain noisy and not satisfying due to the presence of (not physical) phase jumps.

Let us apply the methods to a different interferogram (see Fig. 22 for interferogram *Int2*), in which fringes are visible everywhere. As before, the first two results are obtained with a not filtered image (see images Fig. 23 and Fig. 24), while figures Fig. 25 and Fig. 26 show the results for the 5×5 median-filtered image Fig. 22. Figures Figg. 23, 24, 25, 26 show that, while the *IACRE* output is a continuous map, in both the not filtered and the filtered images the FFT-based output is noisy and not free from phase jumps. This behaviour for the FFT-b output is caused by a strong presence of noise, which could not be completely removed preserving the fringe structure. Instead, the noise seems not disturb the *IACRE* phase-shift computation which produces reasonable results

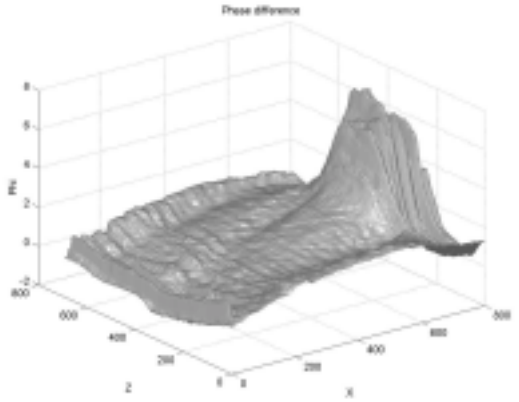

Figure 21: *The phase-shift map (in 2π units) of the Median-filtered (5×5) + Wiener-filtered (5×5)* **Int1** *image Fig. 13.* **FFT method**

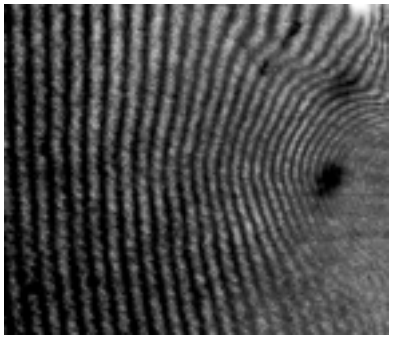

Figure 22: *A sample interferogram* **Int2** *obtained in similar conditions as* **Int1** *but with the probe pulse reaching the plasma at a later time* ($4.3ns$).

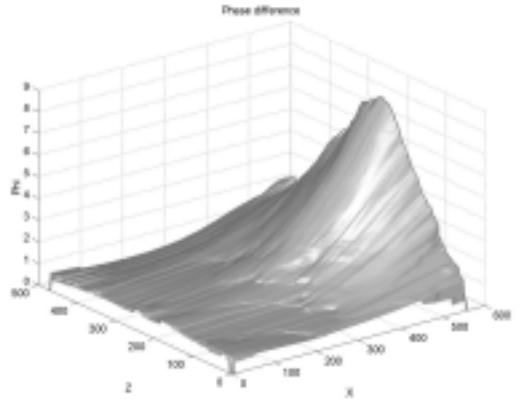

Figure 23: *The phase-shift map (in 2π units) of the of the unfiltered* **Int2** *image Fig. 22.* **CWT method**

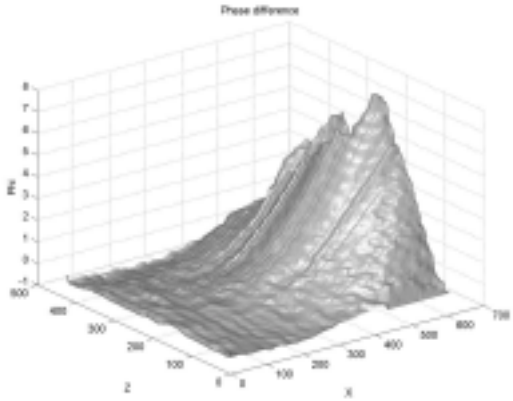

Figure 24: *The phase-shift map (in 2π units) of the not filtered* **Int2** *image Fig. 22.* **FFT method**

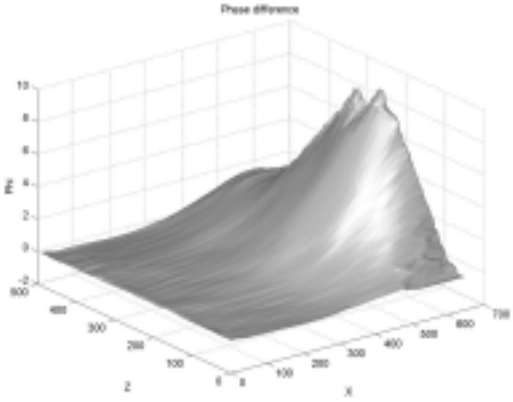

Figure 25: *The phase-shift map (in 2π units) of the of the Median-filtered (5×5)* **Int 2** *image Fig. 22.* **CWT method**

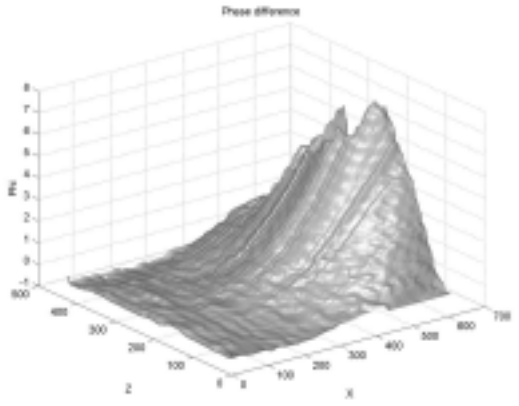

Figure 26: *The phase-shift map (in 2π units) of the Median-filtered (5×5)* **Int 2** *image Fig. 22.* **FFT method**

even with the not denoised image.

To end the comparison between the CWT and FFT based approaches, let us apply the methods to two interferograms *Int 3* (see Fig. 27) and *Int 4* (see figure Fig. 28), where localized effects due to a plasma channel formation are under investigation. The four images Figg. 29, 30, 31 and 32) are referred to the phase-shift maps of the not filtered *Int 3* image and the 3×3 Median filtered $+ 5 \times 5$ Wiener filtered image Fig. 27. From figures Figg. 30 and 32 we can see that the FFT outputs of *Int 3* are satisfying but still noisy, while the *IACRE* outputs are both very accurate and free from noise.

The output of *IACRE* method for the not denoised image of *Int4* is shown in Fig. 33, which should be compared with the FFT-based phase-shift map (figure 34) of the Median filtered + Wiener filtered 3×3 *Int 4* image. Since image *Int 4* is very noisy and presents strong decrease of fringe visibility at the channel boundary, standard FFT method clearly fails in detecting phase-shift map. Instead, the *IACRE* method ($N_v = 24, \omega_0 = 2\pi, \tau = 0.25$) well captures the phase-shift map even in the critical zones at the channel boundary.

Let us conclude this section with some comments about *IACRE* and FFT-based behaviours with sub-optimal images:

- (1) The application of the two techniques to unfiltered (noisy) images led to unsatisfactory

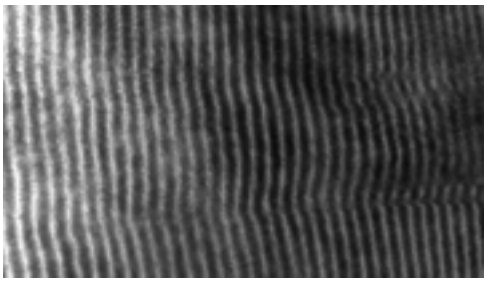

Figure 27: *A sample interferogram* **Int3** *of a channel in a preformed plasma generated by ultra-relativistic laser-plasma interactions with preformed plasmas. The preformed plasma was generated using a similar technique as in the case of* **Int1**. *A relativistically intense laser pulse is then focused in the preformed plasma where it creates a density channel [8]. The probe pulse in this case was* $1ps$ *pulselength* $0.25\mu m$ *wavelength and was timed to reach the plasma* $40ps$ *after the channel forming pulse*

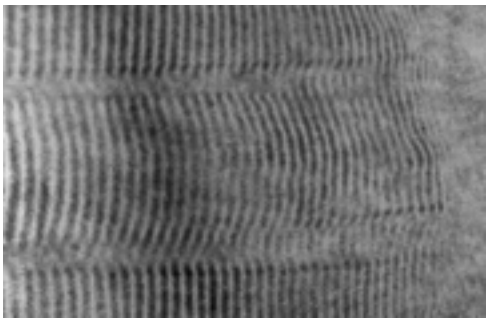

Figure 28: *A sample interferogram* **Int4** *taken in similar conditions as* **Int4** *but with the probe pulse reaching the plasma at a later time with respect to the channel forming pulse* ($60ps$).

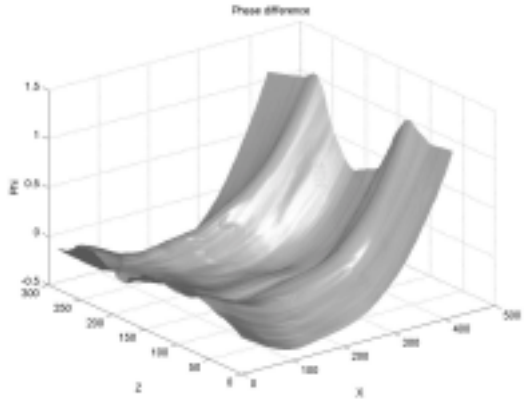

Figure 29: *The phase-shift map (in 2π units) of the not filtered* **Int 3** *image Fig. 27.* **CWT method**

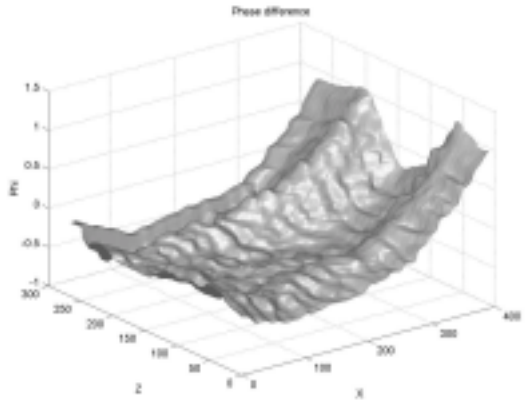

Figure 30: *The phase-shift map (in* 2π *units) of the not filtered* **Int 3** *image Fig. 27.* **FFT method**

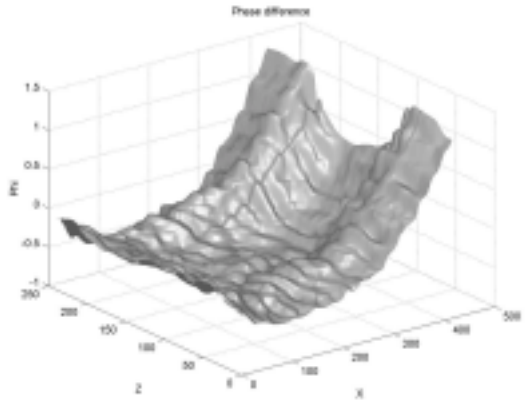

Figure 32: *The phase-shift map (in* 2π *units) of the Median-filtered* (3×3) *+ Wiener filtered* 5×5 **Int 3** *image Fig. 27.* **FFT method**

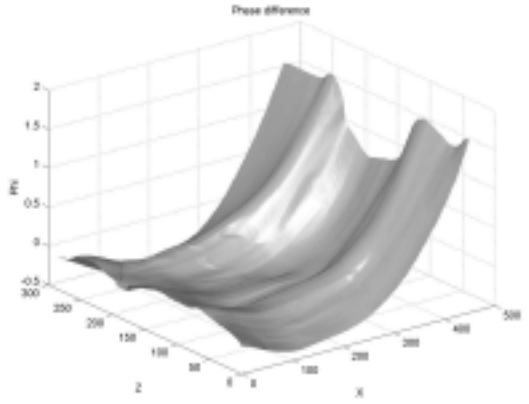

Figure 31: *The phase-shift map (in* 2π *units) of the Median-filtered* (3×3) *+ Wiener filtered* 5×5 **Int 3** *image Fig. 27.* **CWT method**

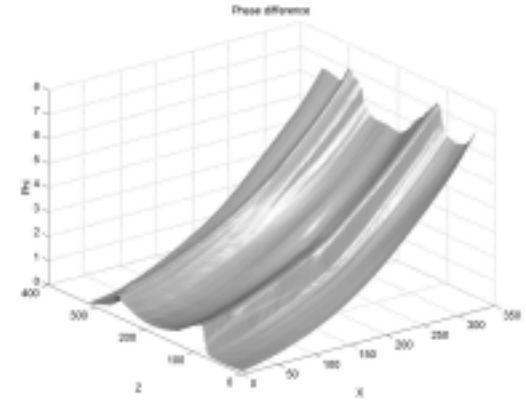

Figure 33: *The phase-shift map (in* 2π *units) of the of the not filtered* **Int4** *image Fig. 28.* **CWT method**

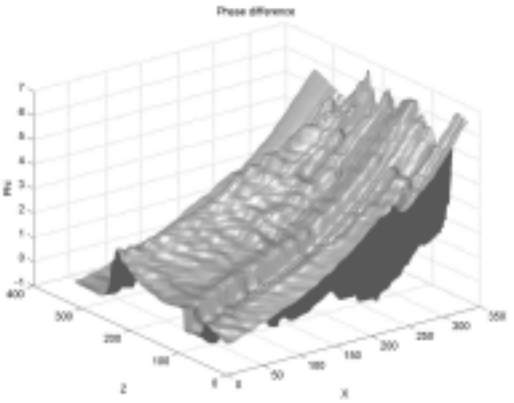

Figure 34: *The phase-shift map (in 2π units) of the of the Median + Wiener 3×3 filtered* **Int4** *image Fig. 28.* **FFT method**

results for FFT-b in interferograms *Int 1, Int 4*. For these images the application of quite strong noise removal filters no not considerably improved FFT-b outputs. The interferogram *Int 2* FFT-b phase-shift maps seems to be more accurate than the output of *Int 1*, but unphysical phase jumps survive to phase-unwrapping procedure. The FFT-b output of interferogram *Int 3* is accurate with both the unfiltered and the filtered images, but still noisy.

- (2) For all the four interferograms *IACRE* phase-shift maps are satisfying and much less noisy than the corresponding FFT-b outputs. With the exception of the interferogram *Int 1*, no visible output improvement is obtained with the prior application of denoising filters to the input images: for most of the images no denoising is needed, **thus saving morphological informations from filtering blurring and other image deformations produced by both linear and non-linear filtering. This is a very important characteristics of our procedure, since it enables an accurate search of small non-uniformity of the phase-shift map which are important to detect the growth of plasma instabilities as filamentation and self-focusing**.

4 The *Integrated Laser-Plasma Interferogram Analyzer* ILPIA software

We describe now briefly the software developed by our group to analyze interferogram images obtained in laser-plasma interaction experiments. It is an integrated software packet running under the MATLAB5 environment consisting by a Graphical User Interface (GUI) and several service routines from which it is possible, starting from a digitized interferogram image, to perform the following operations:

- 1. Definition of a Region of Interest (ROI) image;
- 2. Filtering of the ROI (Median filter, Wiener filter, Background-removal filter and other add-on filters);
- 3. Computation of the phase-shift map with the **FFT-b** method;
- 3. Computation of the phase-shift map with the *IACRE* method;
- 4. Reconstruction of the fringe pattern from the phase-shift map (very useful tool in the result-evaluation step);
- 5. Computation of the density map *via* the Abel Inversion algorithm;
- 6. Standard tools for image-outputs storing.

In Fig. 35 it is shown the **ILPIA** GUI with a ROI in the top image and a *IACRE* intermediate step (the extraction of the CWT map for each z), while in Fig. 36 the GUI aspect of the density computation step, that is the electronic plasma density computed from the phase-shift *via* Abel Inversion, is shown.

5 Conclusions

In this note we have reported the results of a research activity developed by the Laser-Plasma Interaction group with the scope of:

- Improve the standard technique for interferogram analysis;

- Develop an integrated tool running under a PC to analyze digitized interferogram images.

From the comparison between the older FFT-based and the proposed *IACRE* methods outputs for four typical interferograms, emerged that the new tool is considerably more robust than the standard algorithm, especially in analyzing strongly noisy images or interferograms containing a relevant lowering of fringe visibility.

The development of the integrated package *ILPIA* constituted the second goal of the activity. Since the package is flexible and easily to upgrade, more efficient noise filtering routines will be added, and more robust Ridge-extraction procedures will be tested.

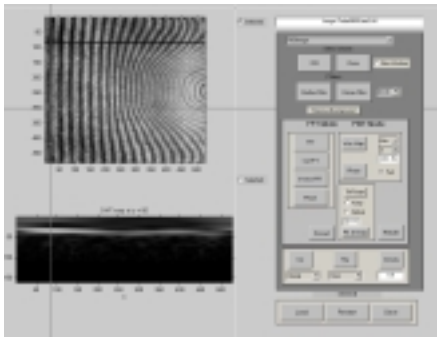

Figure 35: *The Graphical User Interface. Top: ROI of an interferogram image. Bottom: absolute value of the CWT map at* $Z = 85$ *(phase-shift computation step)*

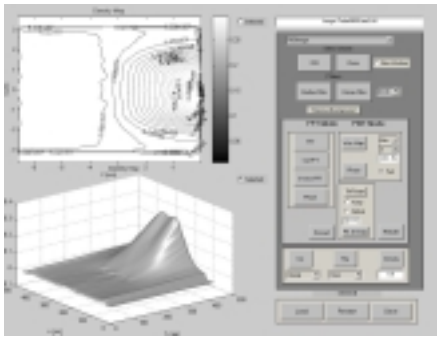

Figure 36: *The Graphical User Interface. Top: Isocontour of the electronic plasma density. Bottom: shaded surface map of the electronic plasma density.)*

Acknowledgments

The authors wish to acknowledge support from the M.U.R.S.T. (Project: "Metodologie e diagnostiche per materiali e ambiente"). One of us (PT) would also thank Guido Buresti (University of Pisa) and Elena Cuoco (I.N.F.N, section of Firenze/Urbino) for useful discussions on Continuous Wavelet Transform.

References

[1] M.G.Nomarski, Journal de la Physique et le Radium **16**, 95 (1955)

[2] R.Benattar, C.Popovics, R.Siegel Rev.Sci.Instrum. **50**, 1583 (1979)

[3] O.Willi, in Laser-Plasma Interaction 4, Proceedings of XXXV SUSSP, St.Andrews, 1988

[4] M.Takeda, H.Ina, S.Kobayashi, J.Opt.Soc.Am. **72**, 156 (1982).

[5] K.A.Nugent, Applied Optics **18**, 3101 (1985)

[6] L.A.Gizzi et al., Phys.Rev. E, **49**, 5628 (1994)

[7] M. Borghesi et al., Phys.Rev. E, **54**, 6768 (1996)

[8] M. Borghesi et al., Phys.Rev.Lett., **78**, 879 (1997)

[9] D. Gabor; *Theory of Communication*, J. Inst. Electr. Eng., London, 93 (III), pp 429-457

[10] J. Morlet, G. Arens, I. Fourgeau and D. Giard; *Wave propagation and sampling theory*, Geophysics, **47**, pp. 203-236

[11] M. Holschneider; *Wavelet: An analysis tool*, Clarendon Press -Oxford (1995)

[12] I. Daubechies; *Ten lectures on Wavelets*, Soc. for Ind. and Applied Mathematics, Philadelphia (1992)

[13] R. Carmona, W.L. Hwang and B. Torresani; *Characterization of Signals by the Ridges of their Wavelet Transform*. paper; IEEE Trans. Signal Processing **45**, vol. 10, p. 2586.

[14] B. Torresani; *Time Frequency and Time Scale Analysis*, abstract in Signal Processing for Multimedia, J. Byrnes Ed. (1999) p. 37-52.

[15] J.M. Innocent and B. Torresani; *A Multiresolution Strategy for Detrection Gravitational Waves Generated by Binary Coalescence*, Submitted to Phys. Rev. D

[16] P. Tomassini; *Uso delle Trasformate Wavelet Continue per lo studio delle emissioni sonore da Autovetture*, Rapporto Ferrari (not publ.), 1998. Contact P. Tomassini, **tomassini@ifam.pi.cnr.it** for details